

## Ultrafast all-electrical universal nanoqubits

David T. S. Perkins<sup>1</sup> and Aires Ferreira<sup>1\*</sup>

*School of Physics, Engineering and Technology and York Centre for Quantum Technologies, University of York, YO10 5DD York, England, United Kingdom*

 (Received 17 July 2023; revised 30 November 2023; accepted 9 January 2024; published 29 January 2024)

We propose how to create, control, and read out real-space localized spin qubits in proximitized finite graphene nanoribbon (GNR) systems using purely electrical methods. Our proposed *nanoqubits* are formed of in-gap singlet-triplet states that emerge through the interplay of Coulomb and relativistic spin-dependent interactions in GNRs placed on a magnetic substrate. Application of an electric field perpendicular to the GNR heterostructure leads to a sudden change in the proximity couplings, i.e., a quantum quench, which enables us to deterministically rotate the nanoqubit to any arbitrary point on the Bloch sphere. We predict these spin qubits to undergo Rabi oscillations with optimal visibility and frequencies in excess of 10 GHz. Our findings open up an avenue for the realization of graphene-based quantum computing with ultrafast all-electrical methods.

DOI: [10.1103/PhysRevB.109.L041411](https://doi.org/10.1103/PhysRevB.109.L041411)

**Introduction.** Quantum computing is a new technological frontier with paradigm-shifting capabilities in fields as diverse as quantum chemistry, cybersecurity, and machine learning [1–3]. Semiconductor platforms for spin-based quantum information processing are a promising path towards realizing stable qubits. Amongst the most prominent spin qubit host systems are quantum dots (QDs) and donors [4], with group-IV semiconductors being at the forefront of current efforts in the field due to their long spin coherence times and scalability potential [5–8]. Leveraging these efforts, recent experiments with silicon qubits have demonstrated one- and two-qubit gate operations yielding fidelities exceeding the thresholds of leading quantum error-correcting codes [9–11], taking spin qubits one step closer to fault-tolerant quantum computing [12].

However, our ability to operate electron spin qubits has predominantly relied upon external magnetic fields to lift the spin degeneracy of the electronic states, which has hindered device miniaturization and set fundamental limits on qubit manipulation speeds [13]. Two methods are routinely implemented to rotate spin qubits: electron spin resonance (ESR) and electric-dipole spin resonance (EDSR). The former requires the use of an oscillating magnetic field to drive resonant transitions between the different spin states of a qubit [14,15]. In contrast, EDSR can only be used in systems possessing a spin-orbit field [16–19], where a constant magnetic field in combination with an oscillating electric field can encourage dipole transitions between the qubit's states, thus simplifying device architectures by allowing for electrically driven qubits [20,21]. To date, the fastest EDSR-driven qubits have been observed in a germanium hut wire displaying coherent

Rabi oscillations at a rate of 540 MHz with a 0.1 T field [19]. Removing the need for external magnetic fields is a critical factor in breaking the gigahertz barrier and improving the energy efficiency of solid-state quantum computers, yet it remains an open question.

The advent of graphene has inspired alternative routes to creating and manipulating quantum bits courtesy of its low dimensionality and exotic Dirac spectrum [22]. Recent studies have had great success in the electrostatic confinement of single electrons in monolayer and bilayer graphene [23–26]. The ability to electrically tune the band gap in bilayer graphene combined with its magnetically addressable valley pseudospin suggests interesting avenues for quantum computing akin to spin-valley qubit operation in silicon [27–29]. Prospects for developing bona fide qubits in bilayer graphene QDs have been boosted with reports of spin lifetimes exceeding 0.2 ms in a 1.9 T magnetic field [30] and single-shot spin readout [31]. Despite these advances, technical challenges in nanofabrication will need to be overcome to operate qubits in the low magnetic field regime, where spin-valley coherence is maximized [32]. More recently, significant advancements in atom-by-atom fabrication of molecular nanographenes have been made that allow for the creation of designer finite graphene nanoribbons (GNRs) with precise shapes and edge morphology [33–36]. Due to their molecular precision, these auspicious GNRs boast spin relaxation times on the order of milliseconds at temperatures as large as 10 K [33], offering exciting prospects for further investigations. A particularly attractive possibility is to encode a logical qubit in sublattice-split states of a finite GNR that are inherently real-space localized, thus providing complementary attributes to the delocalized spin-valley qubits in gated-defined QDs. Atomically precise GNRs may therefore establish the next epoch of quantum computing for qubit encoding via natural quantum confinement.

In this Letter, we propose a type of universal spin qubit that can be manipulated via purely electrical methods (i.e., a universal all-electrical nanoqubit), encoded in

\*aires.ferreira@york.ac.uk

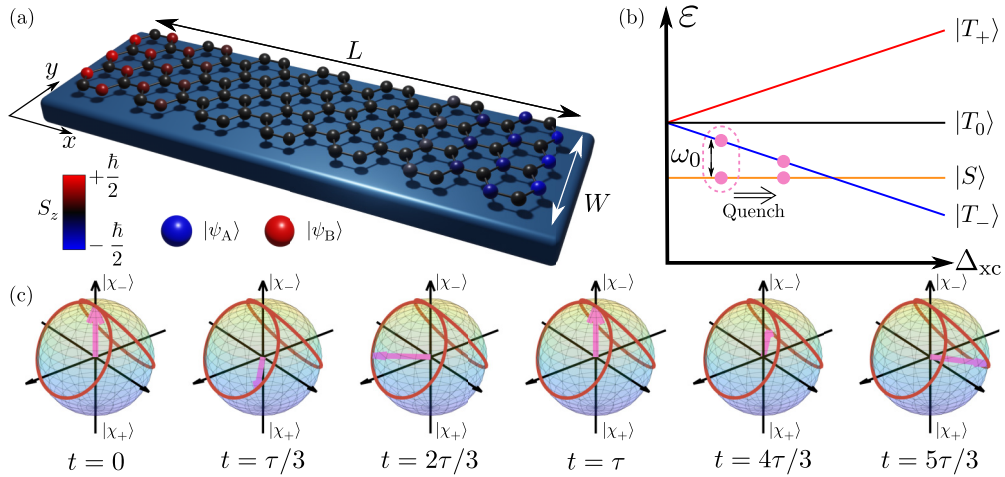


FIG. 1. (a) Schematic of an  $L \times W$  atom GNR placed on a magnetic substrate with sublattice localized states appearing at opposite ends of the GNR. (b) Schematic of how the singlet and triplet energy levels evolve with  $\Delta_{xc}$ . The qubit will be formed from the  $|S\rangle$  and  $|T_-\rangle$  states, with a gap of  $\omega_0$  between them, and is denoted by the pink dashed box. Applying a quench that suddenly increases  $\Delta_{xc}$  shifts the energies of the singlet and triplet, triggering the spin qubit dynamics. (c) An example orbit traversed by the qubit (pink arrow) through the Bloch sphere postquench, with  $\tau = 1/f_R$  being the Rabi oscillation period. The  $|\chi_{\pm}\rangle$  are the ground state ( $-$ ) and excited state ( $+$ ) of the qubit resulting from superpositions of  $|S\rangle$  and  $|T_-\rangle$ .

pairs of quasidegenerate, real-space localized in-gap states that are ubiquitous in zig-zag GNRs, GNRs with tunable extensions, and molecular nanographenes [37–41]. Prototypical real-space localized states, such as edge states, emerge in sublattice-compensated nanographenes and possess well-defined spin and sublattice-pseudospin, stabilized via antiferromagnetic correlations [42,43]. Our scheme utilizes the vast potential of proximity effects to create bespoke nanostructures with optimal relativistic electronic structure realized through graphene’s pairing with other two-dimensional (2D) materials [44–46]. Specifically, atomically thin magnets (e.g.,  $\text{Cr}_2\text{Sn}_2\text{Te}_6$ ) provide an intrinsic time-reversal symmetry breaking mechanism, by which to lift the spin triplet degeneracy, and induce proximity magnetic exchange coupling (MEC) up to 6.8 meV in graphene [47–50]. Furthermore, atomically thin semiconductors in the group-VI dichalcogenide family have been shown to induce Rashba spin-orbit coupling (SOC) as large as 13 meV in graphene [51,52]. Therefore, proximity effects can be exploited to gain all-electrical access to qubit encoding spaces of a naturally confined GNR. What makes our system stand out, as we show below, is that electrical driving of qubit rotation can be achieved using an applied out-of-plane electric field to rapidly change the Rashba SOC and MEC induced by a partner material. Such a quantum quench protocol provides deterministic control akin to the ESR and EDSR approaches, without the need for external magnetic fields. The tunability of proximity effects in graphene nanostructures is shown to easily allow for coherent Rabi oscillations with perfect visibility and frequencies far exceeding the 1 GHz barrier, approaching the terahertz regime in small GNRs. Such nanoqubits are thus predicted to outperform even the fastest group-IV semiconductor-based spin-orbit qubits, with current record Rabi frequencies of 540 MHz in Ge [19]. We furthermore show that the nanoqubits can be detected in a graphene bridge setup similar to Ref. [36] by using a single-shot readout

protocol akin to Refs. [31,53], wherein a charge detector in the form of a secondary QD is used to detect the electrostatic changes due to the loading/unloading of an electron from the proximity-coupled GNR. Graphene nanostructures of this scale have been fabricated using bottom-up methods in a series of recent studies [33–36], wherein long spin lifetimes ( $T_1 \approx 5$  ms and  $T_2 \approx 0.4$   $\mu\text{s}$  at 2 K) were observed which may benefit their ability to host nanoqubits.

*Model.* We consider the class of particle-hole symmetric finite GNR systems whose spinless noninteracting Hamiltonians exhibit a pair of in-gap states [39–41,54] (i.e., quasidegenerate zero energy states),  $|\psi_{\pm}\rangle$ , lying close to and symmetrically about zero energy at  $\varepsilon_{\pm}$ , and that are energetically well separated from all other states. An example of such a system is depicted in Fig. 1(a), which we use as proxy for the quality of the envisaged nanoqubits. From these low-energy states, we can construct two sublattice-localized states,  $|\psi_{A(B)}\rangle = (|\psi_+\rangle \pm |\psi_-\rangle)/\sqrt{2}$  [39], which are further localized at the opposite zig-zag edges of the GNR [see Fig. 1(a)]. In what follows, we refer to these states as quasidegenerate zero energy modes (QZEMs). The effective two-site Hubbard Hamiltonian (see Ref. [40] and Supplemental Material [55]) for a proximitized GNR in terms of the QZEMs is given by

$$\begin{aligned} \tilde{H} = & \sum_{\sigma} (\tilde{t} a_{\sigma}^{\dagger} b_{\sigma} + \tilde{\lambda}_{R,\sigma} a_{\sigma}^{\dagger} b_{\bar{\sigma}} + \text{H.c.}) \\ & + \sum_{v=a,b} [\Delta_{xc}(v_{\uparrow}^{\dagger} v_{\uparrow} - v_{\downarrow}^{\dagger} v_{\downarrow}) + \tilde{U}(v_{\uparrow}^{\dagger} v_{\uparrow} v_{\downarrow}^{\dagger} v_{\downarrow})], \end{aligned} \quad (1)$$

where  $\tilde{t} = (\varepsilon_+ - \varepsilon_-)/2 = \delta/2$  is the QZEM hybridization energy,  $\tilde{\lambda}_{R,\sigma} = \text{sgn}(\sigma)\tilde{\lambda}_R$  is the effective Rashba SOC strength due to interfacial breaking of mirror reflection symmetry,  $\Delta_{xc}$  is the proximity-induced MEC,  $\tilde{U}$  is the effective on-site Hubbard interaction,  $\bar{\sigma} = -\sigma$ , and  $a_{\sigma}^{(\dagger)}$  and  $b_{\sigma}^{(\dagger)}$  annihilate (create) a particle with spin  $\sigma$  in state  $|\psi_A\rangle$  and  $|\psi_B\rangle$ , respectively. For half filling, the two-site model leads

to a six-dimensional Fock space spanned by the basis  $\{|2, 0\rangle, |0, 2\rangle, |\uparrow, \uparrow\rangle, |\downarrow, \downarrow\rangle, |\downarrow, \uparrow\rangle, |\uparrow, \downarrow\rangle\}$ , where the first and second states represent doubly occupied  $A$  and  $B$  sites, respectively, whilst the remainder of the states correspond to the different spin configurations of a single occupation on each site. Recasting  $\tilde{H}$  in this basis, we find that the lowest two eigenstates can be isolated by tuning the MEC [see Fig. 1(b)]. In the limit of vanishing Rashba SOC, these low-lying states can be identified as the spin singlet,  $|S\rangle$ , and spin triplet,  $|T_-\rangle$ , that entangle the spin and sublattice-pseudospin degrees of freedom. It is these states that shall form the nanoqubit. Having a sizable Rashba SOC is crucial to enable resonant transitions between the singlet and triplet. The use of a Rashba SOC generated by an STM tip to manipulate spins in nanographenes via EDSR was discussed in Ref. [39]. However, there are two notable differences between the nanoqubit proposed here and previous work. First, the use of proximity-induced SOC yields extremely large values of Rashba SOC (on the order of 10 meV), which grants easy electrical access to optimal Rabi oscillations through modulation of the proximity couplings via an electric field, as shown below. Second, degeneracies in the qubit-operating manifold are lifted due to the breaking of time-reversal symmetry by MEC, therefore entirely removing the need for external magnetic fields.

Isolating the nanoqubit to first order in the Rashba coupling yields the effective qubit Hamiltonian:

$$\mathcal{H} = -\frac{\omega_0}{2}\sigma_z + g_R\sigma_x, \quad (2)$$

where  $\sigma_{x,z}$  are Pauli matrices,  $\omega_0 = -\Delta_{xc} + (\mathcal{S} - \tilde{U})/2$ ,  $g_R = 8\tilde{t}\tilde{\lambda}_R[\tilde{U} + \mathcal{S}]^{-1}[2 + 32\tilde{t}^2/(\tilde{U} + \mathcal{S})^2]^{-1/2}$ , and  $\mathcal{S} = \sqrt{16\tilde{t}^2 + \tilde{U}^2}$ . From Eq. (2) we can immediately see that the role played by the symmetry-breaking Rashba SOC is to allow transitions between the singlet and triplet manifolds. The qubit manifold is separated from the triplet states  $T_+$  and  $T_0$  by  $\max[|\Delta_{xc}|, |\mathcal{S} - \tilde{U}|/2]$ , depending on whether  $|S\rangle$  or  $|T_-\rangle$  is the ground state.

*Universal qubit control.* The electrical manipulation of single electron spins is traditionally achieved via EDSR [16–19,56], with recent works having realized fast qubits in silicon nanowire quantum dots [16] and hole qubits in Ge [19], as well as predicting Rabi frequencies up to 250 MHz in 2D semiconductors [57]. Here we put forward an alternative approach, a quantum quench, that takes advantage of the superior electrical tunability of atomically thin systems [58–60] to realize all-electrical qubits. By applying a pulse gate voltage across the GNR heterostructure, the effective qubit parameters in Eq. (2) can be efficiently modulated above or below their zero-field values. The resulting change in the Rashba SOC and MEC is sensitive to the choice of materials used to proximitize the GNR, their structural orientation, and the direction of applied field, with variations as large as 10–30% in several candidate materials, such as  $\text{Cr}_2\text{Ge}_2\text{Te}_6$  [50,61]. This fine degree of electrical tunability offers a wide range of possible control quenches achievable within state-of-the-art GNR experimental platforms.

Let us start by considering a system whose MEC and effective Rashba coupling are given by  $\Delta_{xc}^{(1)}$  and  $\tilde{\lambda}_R^{(1)}$ , respectively, for all time  $t < 0$ . The corresponding qubit will then be governed by the Hamiltonian in Eq. (2) with  $\omega_0 = \omega_0^{(1)}$  and

$g_R = g_R^{(1)}$ . We denote the excited state and ground state of this qubit by  $|\chi_{\pm}^{(1)}\rangle$ , respectively. At  $t = 0$  we apply the quantum quench to rapidly change the MEC and Rashba SOC, which in turn changes the parameters of the qubit Hamiltonian,  $\omega_0^{(1)} \rightarrow \omega_0^{(2)}$  and  $g_R^{(1)} \rightarrow g_R^{(2)}$ . Prior to the quench the qubit will be in the ground state  $|\chi_{-}^{(1)}\rangle$ . After the quench, the qubit will be in the time evolving state  $|\psi(t)\rangle = e^{-i\mathcal{H}t}|\chi_{-}^{(1)}\rangle$ , and we find the probability of measuring the qubit in state  $|\chi_{+}^{(1)}\rangle$  to be

$$P(t) = \sin^2\left(\frac{\Delta_2 t}{2\hbar}\right)\sin^2(2\psi_{12}), \quad (3)$$

where  $\Delta_2 = E_{+}^{(2)} - E_{-}^{(2)}$  is the difference in energies of the eigenstates for the postquench system,  $\psi_{12} = \psi_1 - \psi_2$  is the singlet-triplet quench mixing, and  $\psi_{1(2)}$  are the prequench (postquench) singlet-triplet angles of the eigenstates; see Ref. [55] for details on their parameter dependence. From Eq. (3), the Rabi frequency for a quantum quench is readily seen to be  $f_R = \Delta_2/h$ , while the amplitude of the Rabi oscillations is set by  $\psi_{12}$ .

To explore the range of Rabi frequencies and amplitudes that can be achieved in such GNRs, let us parametrize our quench in terms of  $\kappa_R$  and  $\kappa_z$ , where  $\tilde{\lambda}_R^{(2)} = \kappa_R\tilde{\lambda}_R^{(1)}$  and  $\Delta_{xc}^{(2)} = \kappa_z\Delta_{xc}^{(1)}$ . The ranges of possible Rabi frequencies and amplitudes are shown in Fig. 2 for a  $36 \times 7$  atom GNR. We see that a decrease of 15 to 20% in  $\Delta_{xc}$  yields the largest oscillations with amplitudes close to 100%. Interestingly, a change in the Rashba coupling has drastically less impact on the qubit dynamics in comparison to the exchange interaction (see Fig. 2 and Ref. [55]). This is ideal from a practical perspective as it makes our qubit control scheme an effective one-dimensional problem; the MEC quench acts as the primary governing parameter of the qubit evolution in parameter space. Focusing on the region of high amplitudes, we find that the associated Rabi frequencies are in excess of 10 GHz; note that the fastest reported qubit reported to date was observed in Ge quantum dots with a Rabi frequency of 540 MHz [19]. As an example, let us consider a quench with  $\kappa_R = 1.1$  and  $\kappa_z = 0.8$ . In this case we obtain Rabi oscillations with an amplitude of 99.9% and a frequency of 27 GHz. Furthermore, for the choice of parameters listed in Fig. 2, we obtain a singlet-triplet gap of  $\omega_0 = 0.28$  meV, corresponding to a thermal stability of  $T_{st} = 3.2$  K ( $T_{st} = \hbar\omega_0/k_B$ ). Finally, we note that this qubit is universal and can access any point on the Bloch sphere with a specifically chosen quench [55].

The dimensions of the GNR also play a central role in determining the characteristics of these 2D nanoqubits. Specifically,  $\delta$  decreases rapidly as the GNR size is increased, resulting in a more positive singlet energy,  $E_s = (\tilde{U} - \sqrt{4\delta^2 + \tilde{U}^2})/2$ , in larger GNRs, while leaving the  $T_-$  triplet energy,  $E_t = -\Delta_{xc}$ , unaffected. Naturally, the singlet-triplet gap, and thus thermal stability of the qubit, will also change with the GNR size (see Table I). For GNRs with  $E_t < E_s$ , an increase in GNR size will guarantee a larger spin-triplet gap, while for GNRs with  $E_s < E_t$ , the same occurs with a reduction in GNR size. Regardless, the region of optimal amplitude appears to narrow rapidly as the singlet-triplet gap is increased, while still coinciding with smaller Rabi frequencies, thus requiring a higher voltage resolution (required to

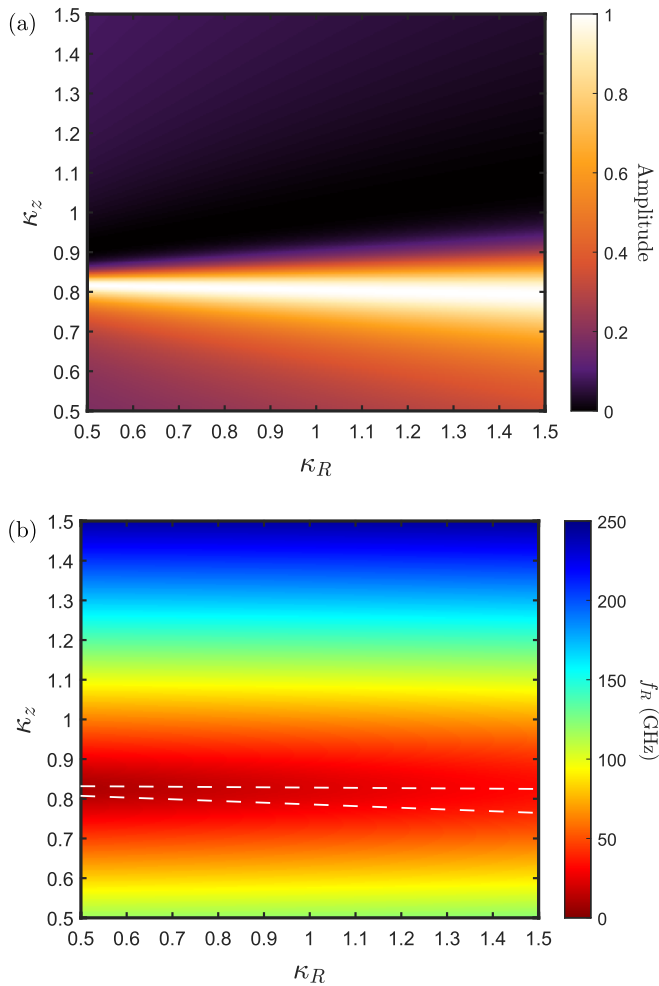


FIG. 2. Resulting Rabi oscillation amplitude (a) and frequency (b) due to a quantum quench in a  $36 \times 7$  atom GNR. The Rabi oscillations can be seen to have frequencies in the range of 1 to 100 GHz for small quenches. The white dashed line in (b) highlights the region of near 100% Rabi amplitudes from (a). The GNR parameters we have used here are nearest-neighbor hopping energy  $t = 2.7$  eV [62], on-site Hubbard repulsion  $U = 2t$  [63–67], Rashba coupling  $\lambda_R^{(1)} = 10$  meV, and  $\Delta_{\text{ic}}^{(1)} = 1.5$  meV. Note that these are bare values characteristic of the entire GNR and are not the effective parameters appearing in Eq. (1). They yield gaps of  $\delta = 18$  meV and  $\Delta = 0.28$  meV with a clear separation of  $|S\rangle$  and  $|T_{-}\rangle$  from the other four states. The corresponding effective parameters are  $\tilde{\lambda}_R = -0.49$  meV,  $\tilde{t} = 9.1$  meV, and  $\tilde{U} = 0.26$  eV. The relations between the effective parameters and the real characteristic parameters can be found in Ref. [55].

hone in on  $\delta\kappa_z$  in Table I) in the experimental apparatus. To explore the large playground of possible GNR dimensions, we analyze how the pre- and postquench qubit Hamiltonian parameters are affected by changes in length along the armchair and zigzag edges in Ref. [55]. Our extensive numerical studies show that the largest amplitudes correspond to the lowest Rabi frequencies for a given GNR, though, these can still be in excess of 10 GHz. Moreover, the largest GNRs will require more extreme quenches to yield optimal oscillations at the cost of smaller frequencies. Specifically, the Rabi amplitude in these cases becomes  $\mathcal{A}_R \simeq (2g_R^{(2)}/\Delta_2)^2 = [2g_R^{(2)}/(hf_R)]^2$ ,

TABLE I. Different GNR dimensions with their corresponding singlet-triplet gaps using the same parameters as in Fig. 2. We give example quenches that yield large amplitude oscillations ( $\geq 99\%$ ) alongside their associated Rabi frequency for  $\kappa_R = 1$ . We consider this case given the lack of sensitivity to changes in the SOC around the high amplitude region. The quench tunability,  $\delta\kappa_z$ , is defined as the range over which the oscillation amplitude is greater than 80%.

$L \times W$	$\omega_0^{(1)}$ (meV)	$\kappa_z$	$\delta\kappa_z$	$f_R$ (GHz)
$36 \times 7$	0.28	0.8000	0.0735	24.9
$44 \times 7$	1.35	0.0975	0.0095	3.44
$52 \times 7$	1.48	0.0116	0.0014	0.49
$16 \times 11$	0.44	0.7050	0.0247	8.95
$28 \times 9$	1.46	0.0287	0.0018	0.66
$36 \times 9$	1.50	$6.1 \times 10^{-4}$	$5.2 \times 10^{-5}$	0.02

meaning that high amplitudes will only be achievable by using quenches that dramatically reduce the MEC (see Table I). Interestingly, this interplay of the Rashba mixing term,  $g_R$ , Rabi frequency, and Rabi amplitude is remarkably reminiscent of the standard Rabi oscillations via periodic driving.

We briefly comment on the effects that defects in the GNR have upon the dynamics of the nanoqubit. Our numerical studies revealed that even the strongest form of disorder in the form of atomically sharp defects (i.e., vacancies) yielded inconsequential changes to the dynamics of the nanoqubit. We attribute this protection to the topological nature of the edge states [68,69] forming the qubit manifold. Similar robustness against point defects has been previously reported for pseudohelical and helical edge states in proximity-coupled GNRs [70,71].

*Detection.* The detection of this nanoqubit can be achieved using a GNR setup similar to Ref. [36] with a charge detection scheme based upon a secondary quantum dot as in Ref. [31]. Specifically, we suggest using two large tapered graphene flakes placed close together with a small gap between their tips, such that the gap lies on a proximitizing substrate. This gap can be bridged placing a large GNR on top of these flakes, such that the GNR extends far into each flake's region. The GNR section bridging this gap will be the finite GNR that may act as a topological QD with the ability to host a nanoqubit. The graphene flakes can be contacted by standard metallic electrodes to allow for the manipulation of their Fermi levels to enable the loading/unloading of electrons from the GNR. Finally, a perpendicular electric field can be applied to the GNR by using a dual-gate setup. To detect the loading/unloading of electrons from the GNR, we propose that a secondary QD be placed in the vicinity of the GNR, such that the change in charge of the GNR leads to a measurable change in the electrostatic potential experienced by the electrons on the secondary QD. By having this detecting QD tuned in to the steep slope of a Coulomb resonance, these changes in the electrostatic potential will be readily detected by the secondary QD. A schematic of this setup is provided in Ref. [55]. To measure the nanoqubit, we propose following the same approach as Ref. [31] but instead of moving the topological QD's energy levels via a plunger gate the Fermi levels of the graphene flakes should instead be moved simultaneously

to emulate moving the GNR energy levels. The step-by-step single-shot nanoqubit readout can be summarized as follows.

- (i) First load two electrons into the GNR's ground state.
- (ii) Raise the graphene flake Fermi energies above the GNR's excited state and then apply the quench using the dual gate.
- (iii) Stop the quench and then lower the graphene flake Fermi energies to lie between the ground state and excited state of the GNR, allowing for the excited state to unload if it is occupied followed by the occupation of the ground state.

*Final remarks.* Let us briefly discuss the effects of spin relaxation and spin decoherence in our setup. The spin relaxation times reported in chemically synthesized nanoribbons are on the order of milliseconds at  $T = 10$  K [33], which is promising. The single-qubit quality factor,  $\mathcal{Q} = \pi f_R T_2$  ( $T_2$  is the decoherence time), is an important figure of merit for our proposal as it estimates the effectiveness of the 2D nanoqubits in performing a successful quantum computation [72]. Our Letter predicts optimal Rabi oscillations ( $P_{\max} \geq 99\%$ ) and  $f_R \approx 100$  GHz in the smallest systems considered [55]. We expect spin-orbit-assisted electron-phonon coupling and hyperfine interactions due to  $C^{13}$  isotopes to be two important limiting factors for  $T_2$ , akin to gate-defined graphene QDs [28,31]. The prominence of spin-phonon relaxation processes is apparent in the time-resolved ESR measurements in GNRs, dominating the spin dynamics at low temperatures relevant for 2D nanoqubit operation [33]. We note that the nanoscale nature of these systems provides an intrinsic protection against spatial fluctuations of chemical potential and proximity couplings common in graphene flakes [73,74] (i.e., spatial variations in  $\lambda_R$  and  $\Delta_{xc}$  due to inhomogeneities in the substrate occur on length scales larger than the GNR), hence reducing decoherence effects originating from the magnetic substrate. The development of a complete microscopic description of these mechanisms in the proximitized GNRs considered here will be an interesting direction for future

research. However, we may garner an insight on the values of  $T_2$  we might expect in these systems, based upon previous studies. With an MEC of 1 meV or larger, reminiscent of a large magnetic field, we anticipate spin-phonon coupling to dominate the spin decoherence rate [75]. For example, taking  $T_2 = 0.4 \mu\text{s}$  from Ref. [33] yields over  $10^4$  coherent single-qubit Rabi oscillations ( $\mathcal{Q} \approx 10^4$ ) for the fastest nanoqubits with  $T_{\text{st}} = 40$  K. Given the fast progress in chemical synthesis of GNRs, we expect near-future systems to achieve even greater quality factors than what we have predicted here.

In conclusion, we have proposed a type of spin-orbit qubit in graphene-based nanostructures that can be rotated using all-electrical methods, yielding coherent Rabi oscillations with Rabi frequencies in excess of 10 GHz that have thermal stability up to order 10 K. The electrical control proposed here is achieved by harnessing the Rashba SOC and MEC induced by the proximitization of finite graphene nanoribbons. The ability to tune these couplings through the use of an out-of-plane electric field unveils a method for qubit manipulation, a quantum quench, which has the potential to open up avenues in other qubit designs. Finally, we showed that this 2D nanoqubit is universal and can be read out using a simple detection scheme similar to the single-shot readout method of Elzerman *et al.* [53]. These ultrafast all-electrical universal nanoqubits are within reach of current bottom-up synthesis methods and offer an alternative route to realizing the first graphene-based qubit. The next challenge for these nanoqubits will be the creation of logic gates using GNR arrays on both a theoretical and experimental front. This is likely to require further advancements in bottom-up synthesis, so that atomically precise GNRs with specified dimensions can be produced with good yield and uniformity.

*Acknowledgments.* The authors acknowledge support from Royal Society (London) under Grants No. URF/R\191021 and No. RF/ER/E\210281.

- 
- [1] M. A. Nielsen and I. L. Chuang, *Quantum Computation and Quantum Information*, 10th ed. (Cambridge University, New York, 2010).
  - [2] Y. Cao, J. Romero, J. P. Olson, M. Degroote, P. D. Johnson, M. Kieferová, I. D. Kivlichan, T. Menke, B. Peropadre, N. P. D. Sawaya, S. Sim, L. Veis, and A. Aspuru-Guzik, *Chem. Rev.* **119**, 10856 (2019).
  - [3] J. Biamonte, P. Wittek, N. Pancotti, P. Rebentrost, N. Wiebe, and S. Lloyd, *Nature (London)* **549**, 195 (2017).
  - [4] S. P. Harvey, *Quantum Dots/Spin Qubits* (Oxford University Press, 2022).
  - [5] J. J. Pla, K. Y. Tan, J. P. Dehollain, W. H. Lim, J. J. L. Morton, D. N. Jamieson, A. S. Dzurak, and A. Morello, *Nature (London)* **489**, 541 (2012).
  - [6] E. A. Laird, F. Pei, and L. P. Kouwenhoven, *Nat. Nanotechnol.* **8**, 565 (2013).
  - [7] N. W. Hendrickx, W. I. L. Lawrie, M. Russ, F. van Riggelen, S. L. de Snoo, R. N. Schouten, A. Sammak, G. Scappucci, and M. Veldhorst, *Nature (London)* **591**, 580 (2021).
  - [8] H. C. Park, J. Han, and N. Myoung, *Quantum Sci. Technol.* **8**, 025012 (2023).
  - [9] X. Xue, M. Russ, N. Samkharadze, B. Undseth, A. Sammak, G. Scappucci, and L. M. K. Vandersypen, *Nature (London)* **601**, 343 (2022).
  - [10] A. Noiri, K. Takeda, T. Nakajima, T. Kobayashi, A. Sammak, G. Scappucci, and S. Tarucha, *Nature (London)* **601**, 338 (2022).
  - [11] M. T. Mądzik, S. Asaad, A. Youssry, B. Joecker, K. M. Rudinger, E. Nielsen, K. C. Young, T. J. Proctor, A. D. Baczewski, A. Laucht, V. Schmitt, F. E. Hudson, K. M. Itoh, A. M. Jakob, B. C. Johnson, D. N. Jamieson, A. S. Dzurak, C. Ferrie, R. Blume-Kohout, and A. Morello, *Nature (London)* **601**, 348 (2022).
  - [12] A. G. Fowler, M. Mariantoni, J. M. Martinis, and A. N. Cleland, *Phys. Rev. A* **86**, 032324 (2012).
  - [13] L. M. K. Vandersypen, H. Bluhm, J. S. Clarke, A. S. Dzurak, R. Ishihara, A. Morello, D. J. Reilly, L. R. Schreiber, and M. Veldhorst, *npj Quantum Inf.* **3**, 34 (2017).

- [14] F. H. L. Koppens, C. Buizert, K. J. Tielrooij, I. T. Vink, K. C. Nowack, T. Meunier, L. P. Kouwenhoven, and L. M. K. Vandersypen, *Nature (London)* **442**, 766 (2006).
- [15] E. Vahapoglu, J. P. Slack-Smith, R. C. C. Leon, W. H. Lim, F. E. Hudson, T. Day, T. Tanttu, C. H. Yang, A. Laucht, A. S. Dzurak, and J. J. Pla, *Sci. Adv.* **7**, eabg9158 (2021).
- [16] A. Corna, L. Bourdet, R. Maurand, A. Crippa, D. Kotekar-Patil, H. Bohuslavskiy, R. Laviéville, L. Hutin, S. Barraud, X. Jehl, M. Vinet, Y.-M. De Franceschi, SNiquet, and M. Sanquer, *npj Quantum Inf.* **4**, 6 (2018).
- [17] F. Borjans, D. M. Zajac, T. M. Hazard, and J. R. Petta, *Phys. Rev. Appl.* **11**, 044063 (2019).
- [18] A. Hosseinkhani and G. Burkard, *Phys. Rev. B* **106**, 075415 (2022).
- [19] K. Wang, G. Xu, F. Gao, H. Liu, R.-L. Ma, X. Zhang, Z. Wang, G. Cao, T. Wang, J.-J. Zhang, D. Culcer, X. Hu, H.-W. Jiang, H.-O. Li, G.-C. Guo, and G.-P. Guo, *Nat. Commun.* **13**, 206 (2022).
- [20] K. C. Nowack, F. H. L. Koppens, Y. V. Nazarov, and L. M. K. Vandersypen, *Science* **318**, 1430 (2007).
- [21] R. C. C. Leon, C. H. Yang, J. C. C. Hwang, J. C. Lemyre, T. Tanttu, W. Huang, K. W. Chan, K. Y. Tan, F. E. Hudson, K. M. Itoh, A. Morello, A. Laucht, M. Pioro-Ladrière, A. Saraiva, and A. S. Dzurak, *Nat. Commun.* **11**, 797 (2020).
- [22] B. Trauzettel, D. V. Bulaev, D. Loss, and G. Burkard, *Nat. Phys.* **3**, 192 (2007).
- [23] M. Eich, F. Herman, R. Pisoni, H. Overweg, A. Kurzmann, Y. Lee, P. Rickhaus, K. Watanabe, T. Taniguchi, M. Sigrist, T. Ihn, and K. Ensslin, *Phys. Rev. X* **8**, 031023 (2018).
- [24] L. Banszerus, S. Möller, E. Icking, K. Watanabe, T. Taniguchi, C. Volk, and C. Stampfer, *Nano Lett.* **20**, 2005 (2020).
- [25] A. Kurzmann, Y. Kleeorin, C. Tong, R. Garreis, A. Knothe, M. Eich, C. Mittag, C. Gold, F. K. de Vries, K. Watanabe, T. Taniguchi, V. Fal'ko, Y. Meir, T. Ihn, and K. Ensslin, *Nat. Commun.* **12**, 6004 (2021).
- [26] R. Garreis, A. Knothe, C. Tong, M. Eich, C. Gold, K. Watanabe, T. Taniguchi, V. Fal'ko, T. Ihn, K. Ensslin, and A. Kurzmann, *Phys. Rev. Lett.* **126**, 147703 (2021).
- [27] P. Harvey-Collard, N. T. Jacobson, C. Bureau-Oxton, R. M. Jock, V. Srinivasa, A. M. Mounce, D. R. Ward, J. M. Anderson, R. P. Manginell, J. R. Wendt, T. Pluym, M. P. Lilly, D. R. Luhman, M. Pioro-Ladrière, and M. S. Carroll, *Phys. Rev. Lett.* **122**, 217702 (2019).
- [28] L. Banszerus, S. Möller, C. Steiner, E. Icking, S. Trelenkamp, F. Lentz, K. Watanabe, T. Taniguchi, C. Volk, and C. Stampfer, *Nat. Commun.* **12**, 5250 (2021).
- [29] R. M. Jock, N. T. Jacobson, M. Rudolph, D. R. Ward, M. S. Carroll, and D. R. Luhman, *Nat. Commun.* **13**, 641 (2022).
- [30] L. Banszerus, K. Hecker, S. Möller, E. Icking, K. Watanabe, T. Taniguchi, C. Volk, and C. Stampfer, *Nat. Commun.* **13**, 3637 (2022).
- [31] L. M. Gächter, R. Garreis, J. D. Gerber, M. J. Ruckriegel, C. Tong, B. Kratochwil, F. K. de Vries, A. Kurzmann, K. Watanabe, T. Taniguchi, T. Ihn, K. Ensslin, and W. W. Huang, *PRX Quantum* **3**, 020343 (2022).
- [32] L. Banszerus, S. Möller, K. Hecker, E. Icking, K. Watanabe, T. Taniguchi, F. Hassler, C. Volk, and C. Stampfer, *Nature (London)* **618**, 51 (2023).
- [33] M. Slota, A. Keerthi, W. K. Myers, E. Tretyakov, M. Baumgarten, A. Ardavan, H. Sadeghi, C. J. Lambert, A. Narita, K. Müllen, and L. Bogani, *Nature (London)* **557**, 691 (2018).
- [34] Z. Chen, A. Narita, and K. Müllen, *Adv. Mater.* **32**, 2001893 (2020).
- [35] M. El Abbassi, M. L. Perrin, G. B. Barin, S. Sangtarash, J. Overbeck, O. Braun, C. J. Lambert, Q. Sun, T. Prechtel, A. Narita, K. Müllen, P. Ruffieux, H. Sadeghi, R. Fasel, and M. Calame, *ACS Nano* **14**, 5754 (2020).
- [36] W. Niu, S. Sopp, A. Lodi, A. Gee, F. Kong, T. Pei, P. Gehring, J. Nägele, C. S. Lau, J. Ma, J. Liu, A. Narita, J. Mol, M. Burghard, K. Müllen, Y. Mai, X. Feng, and L. Bogani, *Nat. Mater.* **22**, 180 (2023).
- [37] M. Fujita, K. Wakabayashi, K. Nakada, and K. Kusakabe, *J. Phys. Soc. Jpn.* **65**, 1920 (1996).
- [38] K. Nakada, M. Fujita, G. Dresselhaus, and M. S. Dresselhaus, *Phys. Rev. B* **54**, 17954 (1996).
- [39] R. Ortiz, N. A. García-Martínez, J. L. Lado, and J. Fernández-Rossier, *Phys. Rev. B* **97**, 195425 (2018).
- [40] R. Ortiz, R. A. Boto, N. García-Martínez, J. C. Sancho-García, M. Melle-Franco, and J. Fernández-Rossier, *Nano Lett.* **19**, 5991 (2019).
- [41] M. Pizzochero and E. Kaxiras, *J. Phys. Chem. Lett.* **12**, 1214 (2021).
- [42] Y.-W. Son, M. L. Cohen, and S. G. Louie, *Phys. Rev. Lett.* **97**, 216803 (2006).
- [43] J. Fernández-Rossier and J. J. Palacios, *Phys. Rev. Lett.* **99**, 177204 (2007).
- [44] M. Offidani, M. Milletteri, R. Raimondi, and A. Ferreira, *Phys. Rev. Lett.* **119**, 196801 (2017).
- [45] J. O. Island, X. Cui, C. Lewandowski, J. Y. Khoo, E. M. Spanton, H. Zhou, D. Rhodes, J. C. Hone, T. Taniguchi, K. Watanabe, L. S. Levitov, M. P. Zaletel, and A. F. Young, *Nature (London)* **571**, 85 (2019).
- [46] J. F. Sierra, J. Fabian, R. K. Kawakami, S. Roche, and S. O. Valenzuela, *Nat. Nanotechnol.* **16**, 856 (2021).
- [47] J. Zhang, B. Zhao, Y. Yao, and Z. Yang, *Phys. Rev. B* **92**, 165418 (2015).
- [48] Y. Wu, Q. Cui, M. Zhu, X. Liu, Y. Wang, J. Zhang, X. Zheng, J. Shen, P. Cui, H. Yang, and S. Wang, *ACS Appl. Mater. Interfaces* **13**, 10656 (2021).
- [49] K. Zollner, M. D. Petrović, K. Dolui, P. Plecháč, B. K. Nikolić, and J. Fabian, *Phys. Rev. Res.* **2**, 043057 (2020).
- [50] K. Zollner and J. Fabian, *Phys. Rev. Lett.* **128**, 106401 (2022).
- [51] D. Wang, S. Che, G. Cao, R. Lyu, K. Watanabe, T. Taniguchi, C. N. Lau, and M. Bockrath, *Nano Lett.* **19**, 7028 (2019).
- [52] Q. Rao, W.-H. Kang, H. Xue, Z. Ye, X. Feng, K. Watanabe, T. Taniguchi, N. Wang, M.-H. Liu, and D.-K. Ki, *Nat. Commun.* **14**, 6124 (2023).
- [53] J. M. Elzerman, R. Hanson, L. H. Willems van Beveren, B. Witkamp, L. M. K. Vandersypen, and L. P. Kouwenhoven, *Nature (London)* **430**, 431 (2004).
- [54] N. V. Tepliakov, J. Lischner, E. Kaxiras, A. A. Mostofi, and M. Pizzochero, *Phys. Rev. Lett.* **130**, 026401 (2023).
- [55] See Supplemental Material at <http://link.aps.org/supplemental/10.1103/PhysRevB.109.L041411> for the derivation of Eqs. (1)–(3), demonstration of qubit universality, more details on the proposed experimental detection scheme, and further analysis of the nanoqubit characteristics for various GNR dimensions.

- [56] E. I. Rashba, *Fiz. Tverd. Tela* **2**, 1224 (1960) [*Sov. Phys. Solid State* **2**, 1109 (1960)].
- [57] M. Brooks and G. Burkard, *Phys. Rev. B* **101**, 035204 (2020).
- [58] B. Yang, M.-F. Tu, J. Kim, Y. Wu, H. Wang, J. Alicea, R. Wu, M. Bockrath, and J. Shi, *2D Mater.* **3**, 031012 (2016).
- [59] D. Sheherbakov, P. Stepanov, S. Memaran, Y. Wang, Y. Xin, J. Yang, K. Wei, R. Baumbach, W. Zheng, K. Watanabe, T. Taniguchi, M. Bockrath, D. Smirnov, T. Siegrist, W. Windl, L. Balicas, and C. N. Lau, *Sci. Adv.* **7**, eabe2892 (2021).
- [60] J. Amann, T. Völkl, T. Rockinger, D. Kochan, K. Watanabe, T. Taniguchi, J. Fabian, D. Weiss, and J. Eroms, *Phys. Rev. B* **105**, 115425 (2022).
- [61] M. Gmitra and J. Fabian, *Phys. Rev. B* **92**, 155403 (2015).
- [62] A. H. Castro Neto, F. Guinea, N. M. R. Peres, K. S. Novoselov, and A. K. Geim, *Rev. Mod. Phys.* **81**, 109 (2009).
- [63] H. Feldner, Z. Y. Meng, A. Honecker, D. Cabra, S. Wessel, and F. F. Assaad, *Phys. Rev. B* **81**, 115416 (2010).
- [64] H. Feldner, Z. Y. Meng, T. C. Lang, F. F. Assaad, S. Wessel, and A. Honecker, *Phys. Rev. Lett.* **106**, 226401 (2011).
- [65] T. O. Wehling, E. Şaşıoğlu, C. Friedrich, A. I. Lichtenstein, M. I. Katsnelson, and S. Blügel, *Phys. Rev. Lett.* **106**, 236805 (2011).
- [66] J. Jung and A. H. MacDonald, *Phys. Rev. B* **84**, 085446 (2011).
- [67] V. M. L. Durga Prasad Goli, S. Prodhan, S. Mazumdar, and S. Ramasesha, *Phys. Rev. B* **94**, 035139 (2016).
- [68] D. J. Rizzo, G. Veber, T. Cao, C. Bronner, T. Chen, F. Zhao, H. Rodriguez, S. G. Louie, M. F. Crommie, and F. R. Fischer, *Nature (London)* **560**, 204 (2018).
- [69] J. Lawrence, P. Brandimarte, A. Berdonces-Layunta, M. S. G. Mohammed, A. Grewal, C. C. Leon, D. Sánchez-Portal, and D. G. de Oteyza, *ACS Nano* **14**, 4499 (2020).
- [70] T. Frank, P. Högl, M. Gmitra, D. Kochan, and J. Fabian, *Phys. Rev. Lett.* **120**, 156402 (2018).
- [71] F. J. d. Santos, D. A. Bahamon, R. B. Muniz, K. McKenna, E. V. Castro, J. Lischner, and A. Ferreira, *Phys. Rev. B* **98**, 081407(R) (2018).
- [72] D. P. DiVincenzo, *Fortschr. Phys.* **48**, 771 (2000).
- [73] A. Locatelli, K. R. Knox, D. Cvetko, T. O. Menteş, M. A. Niño, S. Wang, M. B. Yilmaz, P. Kim, R. M. J. Osgood, and A. Morgante, *ACS Nano* **4**, 4879 (2010).
- [74] I. M. Vicent, H. Ochoa, and F. Guinea, *Phys. Rev. B* **95**, 195402 (2017).
- [75] M. O. Hachiya, G. Burkard, and J. C. Egues, *Phys. Rev. B* **89**, 115427 (2014).